J. Fluid Mech. (1986), *vol.* 173, *pp.* 473–499
Printed in Great Britain

An experiment on boundary mixing: mean circulation and transport rates

By O. M. PHILLIPS, JINN-HWA SHYU AND HAYDEE SALMUN

Department of Earth and Planetary Sciences, The Johns Hopkins University, Baltimore, MD 21218, USA

(Received 10 December 1985)

An experiment is described in which a turbulent boundary layer was generated along a sloping wall of a laboratory tank containing salt-stratified fluid. Initially, the pycnocline separating the upper fresh-water layer from the lower saline layer was relatively thin; it thickened in response to the mixing as the experiment proceeded. Two types of mean circulation developed as a result of the boundary mixing. In the boundary layer, counterflowing mean streams were observed that augmented the diffusion of salt up- and downslope. This augmented dispersion in turn tended to spread the salt beyond the depth range of the pycnocline in the ambient fluid, producing a mean convergence in the boundary layer and intrusions from the layer into the ambient fluid.

The evolving density structure in the ambient fluid was measured by conductivity-probe traverses, from which the net buoyancy flux (or salt flux) and volume flux in the boundary layer were determined. The level of zero volume flux was found to coincide closely with the level of maximum stability frequency N, so that the buoyancy transport across this level was entirely the result of turbulent dispersion in the boundary layer. At other levels, the convective transports up and down contribute significantly. A simple theory provides scaling in terms of the laboratory parameters; in terms of the inferred overall turbulent viscosity ν_e, the buoyancy transport resulting from boundary-layer dispersion was found to be

$$F_B = 0.60 \left\{\frac{\nu_e N(z)}{\sin\theta}\right\}^{\frac{3}{2}} \cos^2\theta,$$

and the intrusion velocity into the ambient fluid is

$$v_I = 0.42 \frac{\nu_e^{\frac{3}{2}}}{N^{\frac{1}{2}} h^2} \frac{\cos^2\theta}{(\sin\theta)^{\frac{3}{2}}},$$

where θ is the angle of the sloping bed. These expressions must become invalid when θ becomes vanishingly small; their application to estuarine and continental slope flows is discussed briefly.

1. Introduction

In his classic paper entitled 'Abyssal recipes', Walter Munk (1966) suggested that oceanic boundary mixing on continental slopes may contribute importantly to the overall vertical mixing in the stratified ocean. Whether the turbulence in the boundary layer is produced by horizontal streaming along the slope or by the breaking of internal waves incident upon it (especially when, with the continuous

oceanic stratification, the slope becomes critical as studied by Wunsch & Hendry 1972 and Ericksen 1985), the effects of the boundary-layer mixing are qualitatively similar. The lateral mixing across the turbulent region reduces the gradients of heat and salt normal to the bed so that the isopycnals are no longer horizontal and an internal secondary circulation must develop in the boundary layer to balance the horizontal buoyancy variations. Moreover, if the distribution $N(z)$ is not constant, the enhanced dispersion up and down the slope will tend to spread out the density gradient in the slope direction, resulting in overall differences between the boundary-layer mean density and that outside; this in turn relaxes to produce entrainment into the boundary layer of the fluid outside or intrusion from the boundary layer into the ambient region. As Wunsch (1970) wrote, following his theoretical discussion of the case $N = \text{const.}$, 'the actual mixing of the ocean interior ... would be due to either slight variations in the vertical temperature gradient or to variations in the angle α of the walls. In either case ... there would be an influx and efflux at various levels of fluid from the interior to the boundary layer where mixing would actually take place.' The experiments to be described in this paper will bear clear witness to the soundness of his intuition.

If boundary mixing is found to be important in the overall oceanic mixing, one would anticipate that it is even more so in estuaries and possibly fjords which have significant mean or tidal flows. Stigebrandt (1976) suggested that internal waves generated tidally at the sill of a fjord would break at its head and mix the thermocline there. He also described a simple qualitative experiment that demonstrated this. In an estuary such as the Chesapeake Bay that is seasonally stratified, without strong internal vertical shear, tidal and shallow in relation to its width, the obvious vertical mixing sources are from the bottom boundary layer and possibly wind mixing from the surface. In a water body of *uniform* depth, surface and bottom mixing lead to a two-layer density distribution with a sharp dividing interface (Turner 1979), quite unlike the diffuse distribution generally observed in the Chesapeake Bay. The inference is that mixing along the gradually sloping bed where it intersects the pycnocline must provide at least powerful competition to simple top and bottom mixing. Olson, Boicourt & Najarian (1982) showed theoretically that localized mixing near the head of a semi-enclosed harbour opening to a two-layered region outside produces a three-layered circulation in the harbour, inwards at the top and bottom and outwards at intermediate depths. He also conducted a few unpublished experiments that confirmed this general tendency. Mixing experiments with an oscillating vertical grid have been described by Thorpe (1982) with a nominally constant density gradient and by Ivey & Corcos (1982) who investigated the two-layer case as well. In some respects, their results and ours are quite similar, the main points of difference arising from the structures of the turbulent boundary layers in the two cases. With an oscillating vertical grid, the thickness of the turbulent boundary layer is not very well defined, as Ivey & Corcos point out, and the interior flow when N is nominally constant is characterized by a pattern of relatively thin horizontal intrusions. The growth of the turbulent boundary layer over a sloping bed, on the other hand, is limited directly by the ambient stratification and its outer edge is better defined; as will be seen later, mean circulations are set up both in the boundary layer and in the interior as fluid is entrained into the boundary layer where the fluid is not stratified and detrained from it where it is. Small-scale intrusions are far less evident.

This paper describes the first results of an experiment designed to investigate these processes. A turbulent boundary layer is generated along a sloping bed in a

laboratory tank filled with water that is stratified by salt. For reasons of scale, it is hardly possible to generate the boundary layer either by horizontal flow along the bed, that is normal to the slope, or by the incidence of internal waves, so that in these experiments it was produced by the controlled oscillation of a rough rubber mat. It will be seen in detail below that the essential driving mechanism of the secondary circulations associated with the overall mixing involves the dispersive characteristics of the turbulent boundary layer, and the boundary layer produced in this way will almost certainly have quantitatively different dispersive characteristics from those of the forced convective flow of a tidal boundary layer or from the turbulence of breaking internal waves. Our primary interest is not centred on the detailed characteristics of this particular experimental boundary layer, but on natural flows, so that the strategy will be first to express our results in terms of the measurable parameters that specify the flow that we generate in the laboratory ($N(z)$, amplitude and frequency of oscillation, etc.), then to measure the local dispersive characteristics of the laboratory turbulence in terms of the same parameters and finally to make the connection. The application to field situations is most direct when the boundary turbulence is generated by mean or tidal streaming along the slope, since we have, or can infer, the basic diffusive properties in the oceanic or estuarine boundary layer with only moderate uncertainty. The application to a turbulent slope layer generated by breaking internal waves is more tenuous since quantitative knowledge of the dispersion behaviour in this case is still absent.

2. Some theoretical considerations

Consider, for the sake of definiteness, the turbulent boundary layer above the sloping bed of a stratified estuary of constant cross-section along the axis. The axial mean velocity U, which may be tidal in origin, will be supposed to vary only slowly, that is over (axial) length- and timescales that are long compared with the boundary-layer thickness and its internal timescales. The variation in slope of the bed will also be supposed small over scales large compared with the boundary-layer thickness. If θ is the angle of inclination of the bed at the depth of the pycnocline and Cartesian axes (x, y, z) are taken respectively in the axial direction, upslope and normal to the bed (see figure 1), the velocity field in the boundary layer can be represented as the sum of the axial mean velocity $U(y, z)$, the mean induced secondary flow $V(y, z)$, $W(y, z)$ together with the turbulent fluctuations $\boldsymbol{u}$. Similarly, the density field is specified as the sum of its mean $\rho(y, z)$ and fluctuation ρ'. The vertical coordinate will be denoted by Z, so that the ambient stability frequency $N = \{-(g/\rho_0)\,\partial\rho/\partial Z\}^{\frac{1}{2}}$.

Since the mean properties of the motion are independent of axial position x, the mean momentum equations in the turbulent boundary layer reduce to

$$V\frac{\partial U}{\partial y}+W\frac{\partial U}{\partial z}=-\frac{1}{\rho_0}\frac{\partial \bar{p}}{\partial x}-\left(\frac{\partial}{\partial y}\overline{uv}+\frac{\partial}{\partial z}\overline{uw}\right), \tag{2.1}$$

$$V\frac{\partial V}{\partial y}+W\frac{\partial V}{\partial z}=-\frac{1}{\rho_0}\frac{\partial \bar{p}}{\partial y}-\frac{\rho}{\rho_0}g\sin\theta-\left(\frac{\partial}{\partial y}\overline{v}^2+\frac{\partial}{\partial z}\overline{vw}\right), \tag{2.2}$$

$$V\frac{\partial W}{\partial y}+W\frac{\partial W}{\partial z}=-\frac{1}{\rho_0}\frac{\partial \bar{p}}{\partial z}-\frac{\rho}{\rho_0}g\cos\theta-\left(\frac{\partial}{\partial y}\overline{vw}+\frac{\partial}{\partial z}\overline{w}^2\right), \tag{2.3}$$

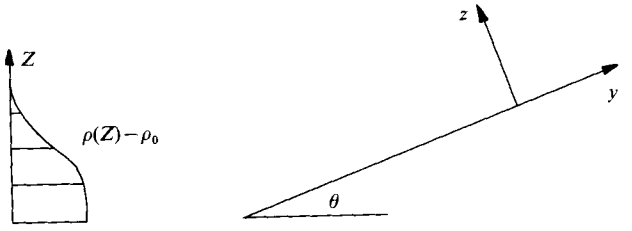

FIGURE 1. A definition sketch.

where the Boussinesq approximation is used and $\bar{p}$ represents the mean pressure. Equations (2.2) and (2.3) can be combined and expressed in terms of the stream function for the mean lateral flow:

$$\frac{\partial(\psi, \nabla^2\psi)}{\partial(y,z)} = \sin\theta\,\frac{\partial B}{\partial z} - \cos\theta\,\frac{\partial B}{\partial y} + \frac{\partial^2}{\partial y\,\partial z}(\overline{v}^2 - \overline{w}^2) + \left(\frac{\partial^2}{\partial z^2} - \frac{\partial^2}{\partial y^2}\right)\overline{vw}, \tag{2.4}$$

where $B = -g(\rho-\rho_0)/\rho_0$ is the mean buoyancy, $V = \psi_z$ and $W = -\psi_y$. The distribution of B is specified by

$$V\frac{\partial B}{\partial y} + W\frac{\partial B}{\partial z} = \psi_z B_y - \psi_y B_z = -\frac{\partial}{\partial y}\overline{bv} - \frac{\partial}{\partial z}\overline{bw}, \tag{2.5}$$

where $b = -g\rho'/\rho_0$.

It is immediately evident that the axial mean flow $U(y,z)$ is not involved directly in the mean balances of the induced secondary flow, specified by (2.4) and (2.5); it does, of course, generate the turbulence which, by mixing and distorting the isopycnal surfaces, produces the secondary flow but it is otherwise uncoupled to it. This observation indicates that the nature and properties of the secondary flow can be modelled and investigated experimentally even if the turbulent boundary layer on the sloping bed is generated by some means other than by axial flow over it; in particular, it may be generated in a laboratory tank filled with stratified fluid and fitted with a sloping rough bed that is agitated to produce the turbulent layer. The detailed forms of parametrization of the mixing characteristics will differ in the two cases but, as mentioned earlier, if the nature and properties of the secondary flow induced in the laboratory can be successfully interpreted in terms of the mixing characteristics of the laboratory boundary layer, then extrapolation to field conditions might be achieved using the mixing properties appropriate there. This extrapolation is considered in §5.

The ambient density field outside the turbulent boundary layer may have a variety of forms both in the laboratory and the field. However, the particular case in which the ambient density gradient is uniform is instructive and will be found useful in interpreting the experimental results. In this circumstance

$$\frac{\partial B}{\partial y} = N^2\sin\theta \tag{2.6}$$

and is constant throughout, where N is the ambient, constant stability frequency. All other mean properties in (2.4) and (2.5) are independent of y, so that the equations reduce to

$$\left.\begin{aligned} 0 &= \sin\theta\left(\frac{\partial B}{\partial z} - N^2\cos\theta\right) + \frac{\partial^2}{\partial z^2}\overline{vw}, \\ N^2\sin\theta\,\psi_z &= -\frac{\partial}{\partial z}\overline{bw}. \end{aligned}\right\} \tag{2.7}$$

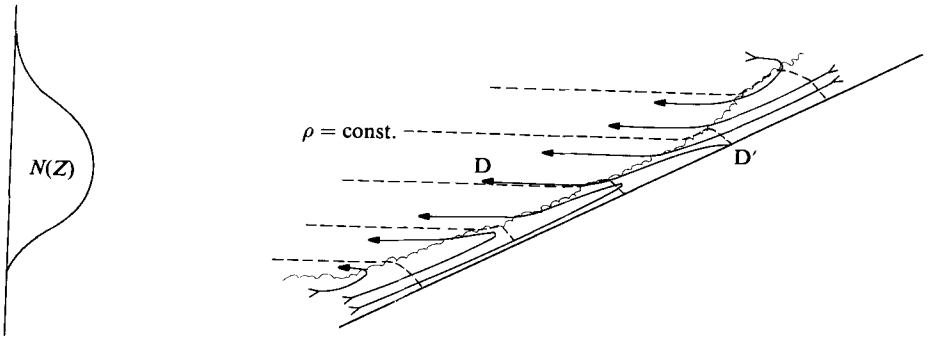

FIGURE 2. A schematic sketch of the isopycnals (dashed lines) and mean streamlines (continuous curves) in the boundary-layer regions, drawn with a good deal of hindsight after a number of dye-tracing observations. Note the dividing mean streamline DD′ across which there is no net volume flux; the mass flux across this mean streamline occurs in the boundary-layer turbulence.

The turbulent buoyancy flux $\overline{bw}$ vanishes both at the bed of the turbulent boundary layer and at its outer edge, $z = \delta$, so that the net mean volume transport

$$F_v = \int_0^\delta \psi_z \, dz \tag{2.8}$$

is not only constant but also vanishes when $N = \text{const}$. In the experiments of Thorpe (1982) and Ivey & Corcos (1982) pertinent to the case, $\theta = 90°$, *local* intrusions emanated from the boundary layer which are certainly associated with variations with depth of the local volume transport in the boundary layer, but about a zero mean – there was no net mean transport in the layer. However, the distribution of the isopycnals sketched in figure 2 and the measurements of figure 5 below imply that fluid in the turbulent boundary layer near its outer edge is denser than the ambient fluid at the same level, while that near the bed at the same value of y is less dense than the outside fluid at *its* level. One would therefore anticipate a net mean downslope flow in the outer regions of the boundary layer and a net upslope flow in the inner regions, the two volume fluxes balancing to ensure that the net flux (2.8) vanishes. This lateral mean shear set up by the turbulent mixing normal to the bed will then enhance the dispersive characteristics of the boundary layer in the y-direction beyond that produced by the turbulence alone, since fluid elements near the top of the layer have a mean drift downslope while those near the bottom drift upslope in mean.

To what extent can the overall lateral dispersive characteristics of the boundary layer be expressed in terms of an enhanced diffusivity? If $N = \text{const}$, the turbulent field is statistically stationary and homogeneous in the y-direction, so that the (Lagrangian) velocity component of a fluid element in the upslope direction is a stationary random function of time as it meanders throughout the depth of the boundary layer. As Batchelor, Binnie & Phillips (1955) showed in the formally analogous case of turbulent flow through a straight pipe, the mean particle velocity is equal to the volume-flux velocity (in the present case zero) and the mean-square displacement from its initial position asymptotically increases linearly with elapsed time:

$$\overline{\{y(t)-y(0)\}^2} \to 2\overline{v_\ell^2}\, t \int_0^\infty S(\tau)\, d\tau = 2\overline{v_\ell^2}\, Tt,$$

where $\overline{v_\ell^2}$ is the mean-square velocity component in the y-direction of fluid elements as they wander throughout the boundary layer and $S(\tau)$ is the corresponding

Lagrangian correlation function. Moreover, an application of the central-limit theorem suggests that the probability distribution of the fluid-particle displacements will approach a Gaussian form when the elapsed time is large compared with the Lagrangian timescale T. Consequently, the net lateral dispersion in the boundary layer might indeed be represented in this case in terms of a diffusivity

$$\kappa_y = 2\overline{v_\ell^2}\,T,$$

which is enhanced by the counterflowing mean circulation, since at instants when the particle finds itself either in the outer or inner regions of the boundary layer, its instantaneous velocity includes both the (Eulerian) mean drift and the turbulent fluctuations.

Consider now the situation in which the stratification in the ambient fluid extends over only a limited depth interval. The enhanced dispersion in the boundary layer, up- and downslope, will tend to diffuse the mean isopycnals in the boundary layer both above the originally stratified depth interval at the top and below it at the bottom. As denser fluid is diffused upslope, it acquires negative buoyancy relative to the ambient fluid at the same level and so tends to sink as a balance develops between the turbulent diffusion upslope and the net convection downslope. The reverse occurs in the lower part of the stratified region so that the mean secondary circulation in the boundary layer has in fact two distinct components – the internal counterflow streaming produced by mixing across the boundary layer and augmenting the dispersion up- and downslope together with a net convergence along the slope that balances this dispersion. As a result of the convergence (as Wunsch anticipated) fluid must enter the turbulent boundary layer at the top and the bottom and leave it at intermediate depths, intruding into the ambient fluid over the interval in which it is stratified, rather as indicated in figure 2. In a tank of finite length (or an estuary of finite width), the streamlines are of course closed and as time goes by the isopycnals in the ambient fluid separate and the density gradients are reduced. Observations of the flow in the experiment and measurements of the volume and mass fluxes are described in more detail below.

3. The model experiment

Experiments were conducted in the tank illustrated in figure 3, with inside dimensions 240 cm long, 13.3 cm wide and 30 cm deep. For each run, it was approximately half-filled with fresh water the temperature of which was allowed to equilibrate with that of the room before a second layer of saline water at room temperature was introduced beneath. The sloping bed was supported by an open frame inclined at an angle of 9.4°. After filling, a thin smooth plastic sheet with rubber seals along each side was slid carefully down the frame to isolate the region below and to the right from the working region above. Finally, the rough bed, the oscillations of which were to generate turbulent boundary layer, was slid down the plastic sheet and attached to a piston drive from an adjustable crank, driven by a variable-speed electric motor through a gear box.

In order to generate a fully turbulent boundary layer, the Reynolds number of the roughness elements during operation had to be as large as reasonably attainable. It was desired to keep the stroke of the oscillation small compared with both the boundary-layer and the pycnocline thicknesses, so that the size of the roughness elements should be as large as possible, though still smaller than both these thicknesses. The material finally chosen for the bed was cut from rubber matting of

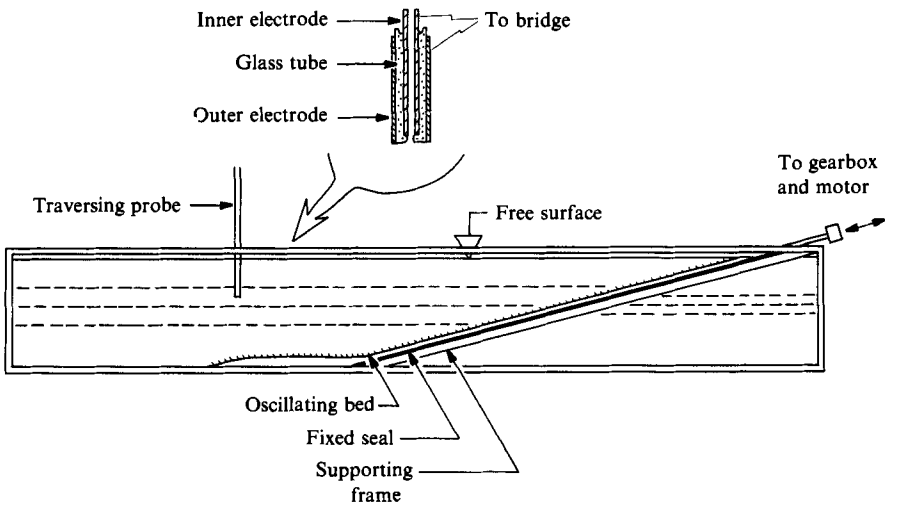

FIGURE 3. A sketch of the apparatus. Dimensions are specified in the text. Details of the probe tip are shown inset.

a kind used inside the front doors of some public buildings, which, though flexible, did not buckle when oscillated. Its upper surface carried a dense pattern of circular florettes or coronets, of diameter 1.1 cm, with 8 conical projections about 0.6 cm high on each; they were arranged in a hexagonal pattern with a spacing of 1.6 cm between centres. In operation, the bed extended from just below the water surface, all the way down the slope and onto the horizontal floor of the tank. Over the bottom 20 cm where the bed was horizontal, the projections were progressively trimmed off so that the bottom leading edge was smooth and did not provide a disturbance site during oscillation.

Qualitative observations of the mixing and circulating flow were made by injection of various dyes and the boundary-layer structure was observed by means of shadowgraph images, all of which were recorded on movie film. More precise quantitative data were gathered by measuring the evolving structure of the internal density field throughout each experimental run, using conductivity-probe traverses. The probe was a modification (and simplification) of a type developed by Dr P. G. Baines of the CSIRO Division of Atmospheric Physics, Aspendale, Victoria, Australia, who kindly provided a set of plans. Our probe needed no precision machining and consisted of a thin-walled glass tube, 0.8 cm in outside diameter, with an end heated until it almost closed, leaving a hole of about 1 mm in diameter at the end. A closely fitting stainless-steel tube was slid down inside the glass tube as far as it would go (almost to the end), and another outside it, also to within 1 mm of the end; these formed the two electrodes of the conductivity probe. The advantages of this type of instrument are first that the electrical current is concentrated in the orifice of the glass tube so that the impedance of the probe is determined by the salinity of the water in the orifice, and the spatial resolution is better than can be obtained from simple point probes. Observations of the response of our instrument when traversing small density steps in the tank indicated a spatial resolution of about 1 mm or better. A second advantage is that the current flow from the electrodes is distributed over a relatively large area so that the overall impedance is much less sensitive to specks of corrosion or dirt that is a point probe, and

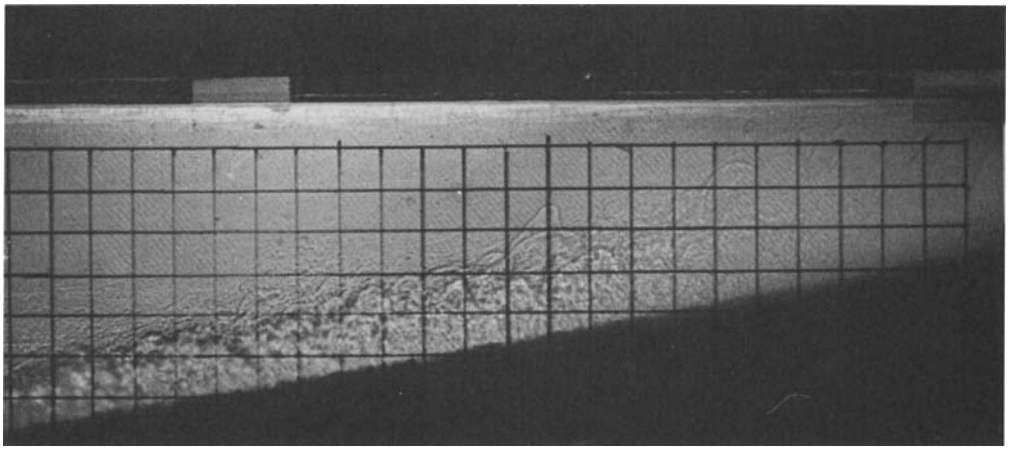

FIGURE 4. A shadowgraph image of the turbulent boundary layer near the top of the pycnocline. Note the residual fine-scale density structure in fluid that has left the boundary layer and is intruding into the ambient fluid.

consequently the instrument holds its calibration much better. In Baines' probe, fluid is slowly withdrawn from the tube as the probe traverses the fluid, but we found that, when traversing downwards at a speed of about 0.1 cm/s, the inner tube filled naturally so that further fluid withdrawal was unnecessary. Upwards traverses, with the inner fluid draining, were of course unusable The impedance of the probe was measured in a bridge and the output recorded continuously on a chart recorder. The system was calibrated before each run (and generally checked afterwards) using standard solutions at the same temperature as the tank and the voltage measurements were digitized from the charts and converted to densities using the measured calibration curve.

In a typical run, the initial pycnocline thickness after the bed had been connected was generally approximately 1 cm. The motor was switched on and the oscillations maintained at a constant frequency (measured by a counter and stop watch, monitored throughout each experiment) and stroke (measured with a micrometer). The turbulent boundary layer developed almost instantaneously, within a second or two, and within a further few seconds the region of the boundary layer containing density fluctuations could be observed in the shadowgraph to creep upwards rather beyond the initially stratified depth range and then come to a state of quasi-stationary equilibrium as the downslope advection developed to oppose the turbulent dispersion. At the outer edge of the boundary layer, the turbulent eddies could be seen to roll downwards as the fluid sought its equilibrium level. Although this outer edge of the vigorous turbulence appeared to remain quite sharp (at least as indicated by the shadowgraph) fluid could be seen (as in figure 4) to leave the boundary layer in the stratified region and intrude into the ambient fluid, carrying with it very fine-scale density structure (fossil turbulence?) that gradually disappeared by molecular diffusion as the fluid moved away. Weak but coherent layers of the kind described by Thorpe (1982) were also observed to move away from the turbulent region, carried by the intruding fluid. Since the frequency of oscillation (and the frequency scale of the eddies) was much larger than the stability frequency N, very few internal gravity waves were generated in the stratified region, though some very low-frequency displacements were observed at the base of the stratified layer as described below.

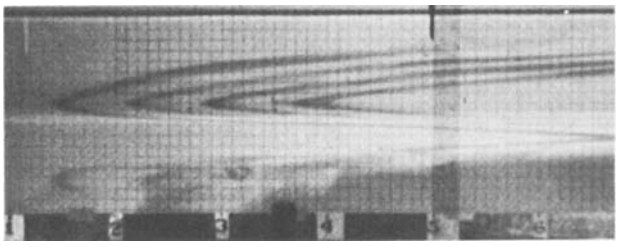

FIGURE 5. Uniformly spaced, initially vertical dye lines in the interior remain with uniform spacing after considerable deformation (horizontal strain about 4), indicating that the horizontal strain rate is independent of x in this region. The sloping bed is to the right and when the photograph was taken the pycnocline, centred at the level of maximum displacement to the left, had thickened substantially.

Also since the rate of strain produced by the intrusions into the interior region was *small* compared with N, the interior motion in the stratified layer was essentially horizontal. Simultaneous multiple dye traces, injected at uniform space intervals down the tank, remained with uniform horizontal spacing as they moved away from the sloping boundary as shown in figure 5, and measurements from the films confirmed that the horizontal velocity at a given depth varied linearly with distance from the far end of the tank. The (very small) vertical velocities in the interior were then independent of horizontally position and the isopycnals remained horizontal, though spreading out vertically in response to the intrusions. In the boundary layer adjacent to the lower part of the pycnocline, dye showed the fluid to move inwards and then upwards along the bed before it ultimately intruded into the interior region. Because the oscillating bed continued below the pycnocline, the lower, constant-density region was also weakly turbulent – traces of large lethargic eddies could be seen in the shadowgraph images to impinge upon the lower side of the pycnocline for a horizontal distance of 10 or 15 cm beyond the vigorously turbulent region, but they did not seem to produce measurable entrainment.

The mean circulation, in which the upper and lower unstratified fluid was drawn into the boundary layer, mixed and re-intruded into the stratified region, developed rapidly, within several seconds of the start of each experiment, and continued steadily throughout the experiment, gradually modifying the density structure during the subsequent 60 or 90 minutes. The experiment was concluded when the density of the initially fresh water at the top of the tank began to increase from its initial value. Conductivity-probe traverses of the interior fluid were made at intervals, initially of 4 to 5 minutes but lengthening to 12 or 15 minutes as the experiment proceeded, time intervals being measured between the instants that the probe passed through the region of maximum density gradient. A typical set of profiles obtained from the chart recorder in a single experiment is shown in figure 6. An astonishing feature of these profiles is that, very closely, they all pass through the single point at which the density gradient is a maximum or where $\partial N/\partial Z = 0$ in the interior, Z being vertically upwards. This observation implies that the isopycnal surface in the interior at this level remains at a constant height throughout the experiment, so that the net volume flux in the boundary layer must vanish at this particular depth. The considerations of the previous section show that volume flux will vanish when $\partial N/\partial Z = 0$ everywhere; apparently this remains true when the density gradient is only locally constant. Indeed, the set of profiles looks remarkably equivalent to simple vertical diffusion, even though they are the end

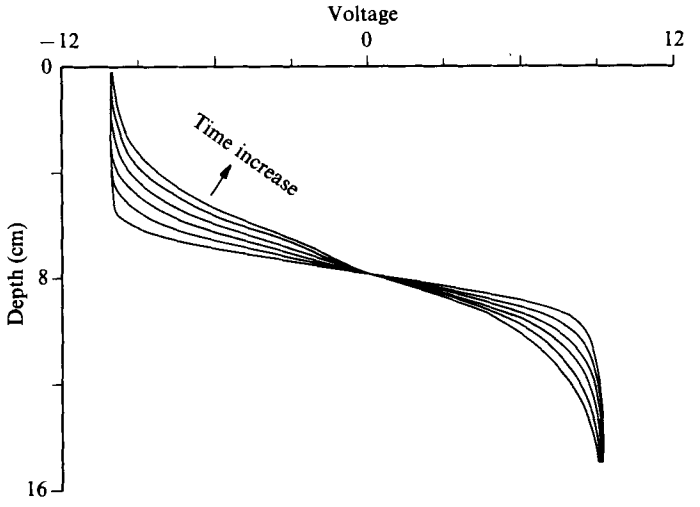

FIGURE 6. A representative sequence of profiles (experiment 19) redrawn after digitization from the chart recorder. Increasing voltage indicates increasing density.

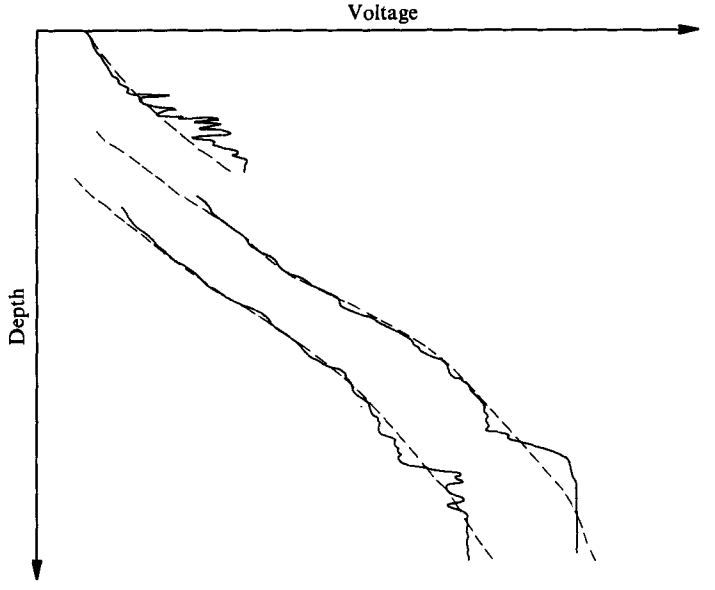

FIGURE 7. Probe traverses into the turbulent boundary layer. Each set represents profiles taken before (the broken lines) and after (the continuous lines) the oscillating bed was switched on. The top pair were obtained in the upper part of the pycnocline and the lower two pairs, displaced vertically downwards in the figure, were taken further downslope, below the point where the maximum value of N intersected the slope.

result of a rather complicated set of boundary-layer mixing processes and induced circulations. Closer examination indicates that the analogy with simple diffusion is not quite precise, though it may be a useful approximation in some circumstances. This is described in detail below.

A few traverses were made with the conductivity probe into the turbulent boundary layer itself, though care had to be taken to avoid contact with the oscillating bed. Three representative records are shown in figure 7. In each case, the

Operating parameters					
				Initial density (g/cc)	
Experiment	ω (rad/s)	a (cm)	Range of $N_{\max}$ (rad/s)	Top	Bottom
15	43.27	0.386	5.85–3.58	0.999	1.061
16	44.40	0.253	4.64–2.99	0.999	1.061
17	51.55	0.241	4.62–3.23	0.999	1.059
19	30.21	0.371	4.82–3.36	0.999	1.061
20	42.38	0.507	3.48–2.60	0.999	1.040

TABLE 1.

profile was measured with the bed and the fluid at rest, after which the motor was switched on and a second profile taken immediately, giving a traverse in space–time as the probe moved down into the boundary layer. Above the turbulent boundary layer, the differences between the two profiles are small, but as soon as the probe encounters the turbulent eddies at the outer edge, positive excursions in voltage, indicating denser fluid, without corresponding negative excursions, are evident. The average density of the turbulent fluid at the outer edge is therefore greater than in the ambient fluid at the same level, as sketched in figure 2. Deeper in the boundary layer, the fluid becomes well mixed and the magnitudes of the excursions generally decrease, though we were unable to approach the bed itself very closely.

4. Quantitative results

Twenty-five experimental runs were conducted, some of which were exploratory or devoted primarily to dye tracing, photography or boundary-layer-thickness measurements. Satisfactory series of conductivity profiles were obtained in five runs, the pertinent operating parameters being specified in table 1. Twenty-eight profiles were analysed in detail.

In order to find the appropriate scaling parameters for the experiment, guidance was provided by the following simple analysis. As described previously, the boundary-layer flow over the range of depth occupied by the pycnocline consisted of the vigorous turbulence that induced the mean up- and downslope boundary-layer streaming, together with the overall convergence along the slope the volume transport of which changed sign very near the depth of maximum N. If one takes a local frame of reference moving with the mean velocity of the convergent flow at a certain depth, since the scales of variation along the boundary layer are large compared with the boundary-layer thickness, the primary balances are still as specified by (2.7). In the mean vorticity equation, the second derivative of the Reynolds stress balances the gradient of the mean buoyancy distribution in the boundary layer:

$$-\frac{\partial^2}{\partial z^2}\overline{vw} = \sin\theta\left(\frac{\partial B}{\partial z} - N^2\cos\theta\right), \tag{4.1}$$

where $\partial B/\partial z$ is the gradient normal to the wall and $N^2\sin\theta$ that along the wall. In the buoyancy field there is a close balance between the gradients of the turbulent flux normal to the wall and the convective flux along the wall, which integrates to

$$N^2\sin\theta\,\psi(z) = -\overline{bw} \tag{4.2}$$

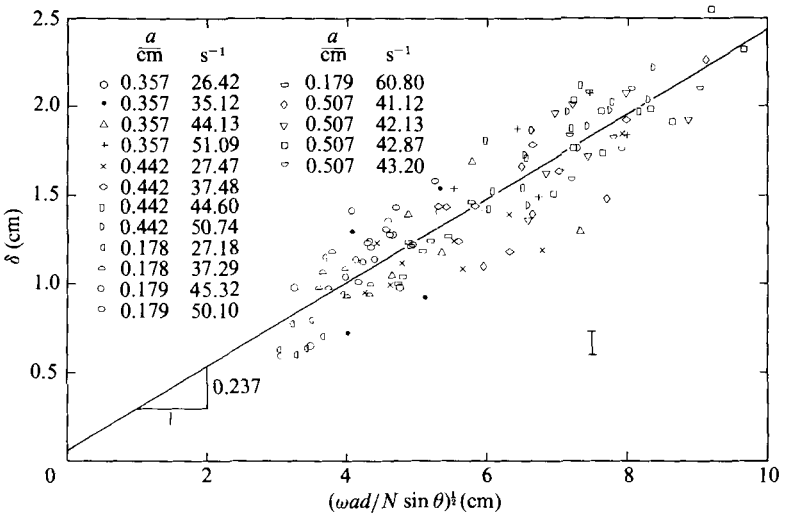

FIGURE 8. Measurements of the height of the outer edge of the boundary layer above the top of the roughness elements.

since $\psi = 0$, $\overline{bw} = 0$ at $z = 0$. Now, in the part of the turbulent boundary layer over the range of depths occupied by the pycnocline, the size of the largest eddies is governed by the spacing d (0.8 cm) of the roughness elements and their velocity scale is proportional to ωa, where ω is the frequency and a the amplitude of the oscillation. For scaling purposes, then, one might represent the diffusive properties of the turbulence in terms of an eddy viscosity ν_e and diffusivity κ_e of the form

$$\nu_e, \kappa_e \propto \omega a d. \tag{4.3}$$

Outside the range of depth over which the ambient fluid is significantly stratified, the boundary-layer growth is much less constrained by the buoyancy effects and is thicker, the scales increasing with distance from the wall, but a constant eddy viscosity and diffusivity seemed to be adequate approximations for the central region, at least for these scaling purposes. Consequently, if

$$-\overline{vw} = \nu_e \frac{\partial V}{\partial z} = \nu_e \frac{\partial^2 \psi}{\partial z^2}$$

and

$$-\overline{bw} = \kappa_e \frac{\partial B}{\partial z},$$

then (4.1) and (4.2) give

$$\frac{\partial^4 \psi}{\partial z^4} + \frac{N^2 \sin^2 \theta}{\nu_e \kappa_e} \psi = -\frac{N^2 \cos\theta \sin\theta}{\nu_e}, \tag{4.4}$$

with homogeneous boundary conditions on ψ at $z = 0$ and as $z \to \infty$. The only lengthscale that appears in this specification is obtained by the proportionality of the first two terms in this equation, so that the boundary-layer thickness in the pycnocline region is expected to be of the form

$$\delta \propto \left(\frac{\nu_e \kappa_e}{N^2 \sin^2 \theta}\right)^{\frac{1}{4}} \propto \left(\frac{\omega a d}{N \sin\theta}\right)^{\frac{1}{2}}. \tag{4.5}$$

The scale of the stream function associated with the counterflowing boundary-layer circulation is given by the proportionality of the last two terms in (4.4):

$$\psi_{\text{scale}} = \kappa_e \cot\theta. \tag{4.6}$$

A test of the scaling (4.5) for the boundary-layer thickness is exhibited in figure 8. Movie film was taken of the shadowgraph images of the turbulent boundary layer for a range of values of ω, a and N; d and θ being fixed throughout the experiment. A frame-by-frame analysis of the film gave measurements of the instantaneous thickness of the boundary layer from the top of the roughness elements to the sharp, convoluted outer edge, about eight realizations being taken for each point and the readings averaged. Since, in the ambient field, N varied somewhat over the depth interval represented by the boundary-layer thickness, the values used in plotting figure 8 were taken as the mean of those at the levels of the top and the bottom of the boundary layer. There is, nonetheless, a considerable degree of scatter in the results since the instantaneous thickness of the actively turbulent region fluctuated considerably, but the measured thicknesses do seem to scale according to (4.5) with a virtual origin (as $\omega ad/N \to 0$) that is not significantly different from zero. (An initial attempt based on a simple energy argument to scale δ as proportional to $\omega a/N$ failed; the cloud of points was clearly curved and the best-fit straight line gave a large positive virtual origin, which does not make sense as $\omega a/N \to 0$.) A least-squares fit to the data of figure 8 gives

$$\delta = \left\{0.24\left(\frac{\omega ad}{N\sin\theta}\right)^{\frac{1}{2}} + 0.14\right\} \text{cm}. \tag{4.7}$$

The measurements of the evolution of the density field in the interior enabled the buoyancy flux along the turbulent boundary layer to be found. From (4.2) in the form

$$\kappa_e \frac{\partial B}{\partial z} = N^2 \sin\theta\, \psi(z),$$

the scale of the buoyancy variations across the boundary layer is given by

$$N^2 \sin\theta\, \psi_{\text{scale}}\, \delta/\kappa_e = N^2\delta\cos\theta,$$

making use of (4.6). The counterflowing mean velocities in the boundary layer scale as $\delta^{-1}\psi_{\text{scale}} = \delta^{-1}\kappa_e \cot\theta$, so that the net convective buoyancy transport produced by the boundary-layer streaming is proportional to

$$(N^2\delta\cos\theta)(\delta^{-1}\kappa_e\cot\theta)\,\delta = \frac{\kappa_e N^2\delta\cos^2\theta}{\sin\theta}. \tag{4.8}$$

The buoyancy transport down the slope produced by the turbulence *alone* in the absence of streaming is $\kappa_e \delta\, \partial B/\partial y \approx \kappa_e N^2\delta\sin\theta$ which, when θ is small, is much less than (4.8). In Thorpe's (1982) experiment with a vertically oscillating wall, $\theta = 90°$ and (4.8) vanishes, but in the present case, with a small slope, the induced secondary streaming augments considerably the ability of the boundary layer to diffuse salt upslope. The overall diffusive transport in the boundary layer upslope is therefore dominated by the contribution (4.8) and can be represented as

$$F_B = -K\delta\frac{\partial B}{\partial Z}, \tag{4.9}$$

where

$$K = \frac{\kappa_e\cos^2\theta}{\sin\theta} \propto \frac{\omega ad\cos^2\theta}{\sin\theta}. \tag{4.10}$$

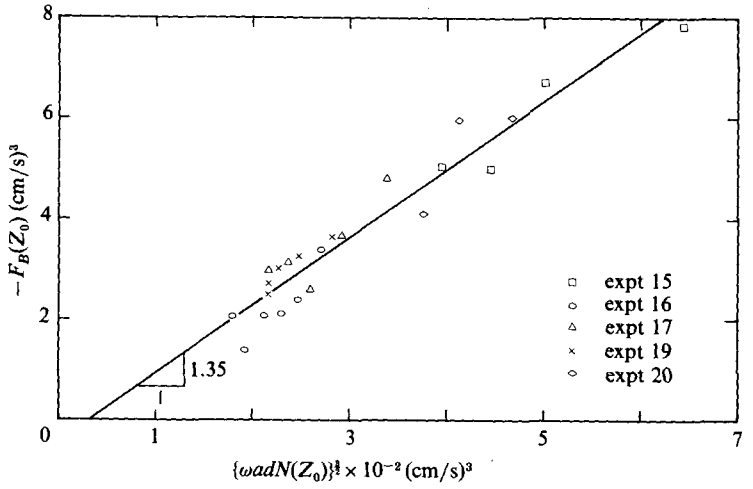

FIGURE 9. Measurements of the buoyancy transport across the height Z_0 of zero volume flux, scaled according to equation (4.11).

The internal boundary-layer transport F_B is, however, not simply proportional to the gradient $\partial B/\partial Z$ since the boundary-layer thickness δ also depends on N; from (4.5) and (4.9),

$$F_B \propto -\left(\frac{\omega a d N}{\sin\theta}\right)^{\frac{3}{2}} \cos^2\theta. \tag{4.11}$$

The total transport of buoyancy across a given level is the sum of this and the convective transport associated with the overall convergence flow along the slope of the boundary layer as a whole but, as illustrated in figure 6, the stagnation point of this component of the flow, the point where the net volume flux vanishes, coincides closely with the depth where N is a maximum. Consequently at *this* level, Z_0 say, the total transport of buoyancy is given by (4.11), an expression that can be tested by the experiments. At any instant t_1, the total mass of fluid in the tank above Z_0 is

$$M(t_1) = \int_{Z_0}^{Z_T} \rho(Z, t_1)\, L(Z)\, \mathrm{d}Z,$$

where Z_T represents the height of the free surface and $L(Z)$ is the length of the working area from the sloping bed to the vertical endwall. (The fraction of $L(Z)$ occupied by the boundary layer was only 1 or 2%.) The change in total mass above Z_0 between traverses at times t_1 and t_2 is therefore

$$\Delta M = M(t_2) - M(t_1) = \int_{Z_0}^{Z_T} \{\rho(Z, t_2) - \rho(Z, t_1)\}\, L(Z)\, \mathrm{d}Z, \tag{4.12}$$

and the mean total transport of buoyancy across the level Z_0 is

$$F_B(Z_0) = \frac{-g\Delta M}{\rho_0(t_2 - t_1)}.$$

The integral in (4.12) was calculated from the digitized density profiles using Simpson's rule and the results are shown in figure 9. In the estimation of N at the point of zero volume flux, the averages of the three adjacent values found from the density profiles were used to avoid undue reliance on a single pair of digitized points.

This figure indicates that the transport of buoyancy along the boundary layer at the depth of zero flux can be represented adequately by

$$F_B(Z_0) = -1.35 \times 10^{-2} \{\omega a d N(Z_0)\}^{\frac{3}{2}}, \tag{4.13}$$

the coefficient being found by a least-squares fit through the origin. If the slope factors in (4.11), which could not be varied in this set of experiments, are included,

$$F_B(Z_0) = -8.9 \times 10^{-4} \left\{\frac{\omega a d N(Z_0)}{\sin\theta}\right\}^{\frac{3}{2}} \cos^2\theta. \tag{4.14}$$

The overall diffusion coefficient K_y for boundary-layer dispersion along the slope is defined so that

$$F_B(Z_0) = -K_y \delta \frac{\partial B}{\partial y} \approx -K_y \delta \sin\theta N^2$$

and

$$K_y \approx \frac{-F_B}{N^2 \delta \sin\theta}$$

$$= 3.8 \times 10^{-3} \cot^2\theta \, (\omega a d). \tag{4.15}$$

It is interesting to compare these results for the buoyancy transport with those obtained by Ivey & Corcos (1982) with a vertical grid. A best-fit representation of their data is given as

$$F_B \propto \omega^{1.6} a^{2.7} N^{1.52},$$

in which the dependence on ω and N is virtually the same as our (4.13) in spite of the different geometries involved. This fitting of their data is however independent of the grid scale, $a^{2.7}$ replacing the factor $(ad)^{\frac{3}{2}}$ in (4.13). In both sets of experiments d was fixed and the range of values of a that could be used varied only by a factor of 2 so that it is difficult to distinguish between the two on the basis of these transport measurements alone. At the heart of the matter is the proper specification of the turbulent lengthscale in the mechanically driven boundary layer; our observations indicate it to be approximately d in the sloping boundary layer (when $d > a$, as in both sets of experiments) while the expression above implies that it is proportional to a. In any event, an important difference between the two sets of experiments that makes quantitative comparison difficult is that, in the sloping boundary layer, the dispersion along the bed is dominated by the internal counterflowing circulation, and this vanishes in the case of a vertical wall, leaving only the dispersion by the turbulence itself.

We shall return to the distribution of buoyancy flux with Z later; let us now consider the volume fluxes associated with the secondary flow convergence. In the boundary layer, the mean buoyancy distribution changes only slowly over the timescales ω^{-1} and N^{-1} that characterize the turbulence; it is quasi-stationary under the combined influence of the net turbulent dispersion along the layer and the overall convergence:

$$\overline{V} \frac{\partial \overline{B}}{\partial y} \approx K_y \frac{\partial^2 \overline{B}}{\partial y^2},$$

where $\overline{V}$ is the mean velocity of the convergence (positive upslope) and $\overline{B}$ the mean buoyancy across the layer. Since throughout the experiments with an initially thin pycnocline, the distributions of $N^2(Z)$ remained fairly Gaussian (figure 10), the mean convergence velocity in the stratified region opposing the dispersion should be approximately a linear function of y:

$$\overline{V} = -\alpha y,$$

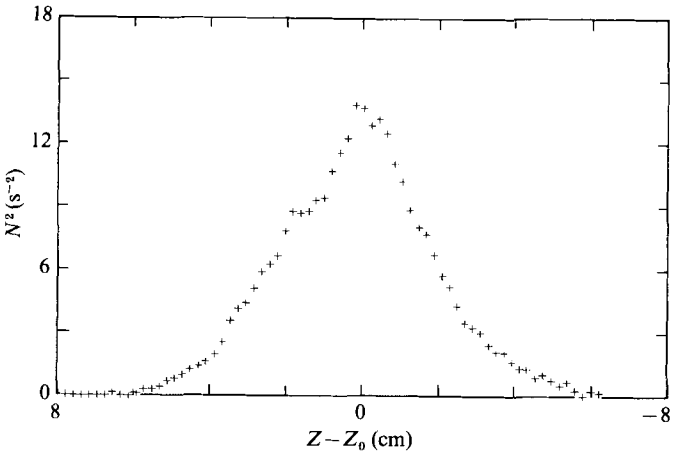

FIGURE 10. A typical profile of $N^2(Z)$ midway through an experiment (number 16, profile 5).

where $\alpha = 2K_y/l^2$, l being the half-width of the stratified region in the boundary layer measured along the sloping wall. We define the half-thickness h of the pycnocline in the ambient fluid as

$$h^{-1} = 2\left(\frac{\partial\rho}{\partial Z}\right)_{\max}\Big/\Delta\rho, \tag{4.16}$$

where $\Delta\rho$ is the overall density difference and the maximum gradient is estimated as the largest mean over three adjacent digitized values. Since the stratification in the boundary layer extends over a rather larger depth range than in the ambient fluid,

$$l \gtrsim \frac{h}{\sin\theta}. \tag{4.17}$$

Since h^{-1} decreased as each experiment proceeded, the means were taken for each successive pair of profiles. The net volume transport in the boundary layer is then expected to be of the form

$$F_v \approx \overline{V}\delta = \frac{2K_y y\delta}{l^2} \lesssim \frac{2K_y\delta(Z-Z_0)\sin\theta}{h^2}. \tag{4.18}$$

With use of the expressions (4.15) and (4.7), neglecting the virtual origin, this can be written in the non-dimensional form

$$\frac{F_v N^{\frac{1}{2}} h}{(\omega a d)^{\frac{3}{2}}} = A\frac{\cos^2\theta}{(\sin\theta)^{\frac{3}{2}}}\frac{Z-Z_0}{h}, \tag{4.19}$$

where $A \lesssim 1.7\times10^{-3}$. With the angle $\theta = 9.4°$ used in these experiments, the proportionality factor is expected to be somewhat less than 2.5×10^{-2}, though in view of the approximations such as (4.17) no more than order-of-magnitude accuracy can be anticipated in the numerical value of the coefficient. Nevertheless, (4.19) does suggest how measurements of F_v should be scaled for the different values of N, h, ω and a used in the experiments, and it is of interest to see how well the results collapse when plotted in this way.

The boundary-layer volume transport F_v was balanced by an equal vertical transport but of opposite sign in the interior region, and since mixing was confined to the boundary-layer region this could be measured by the vertical displacements

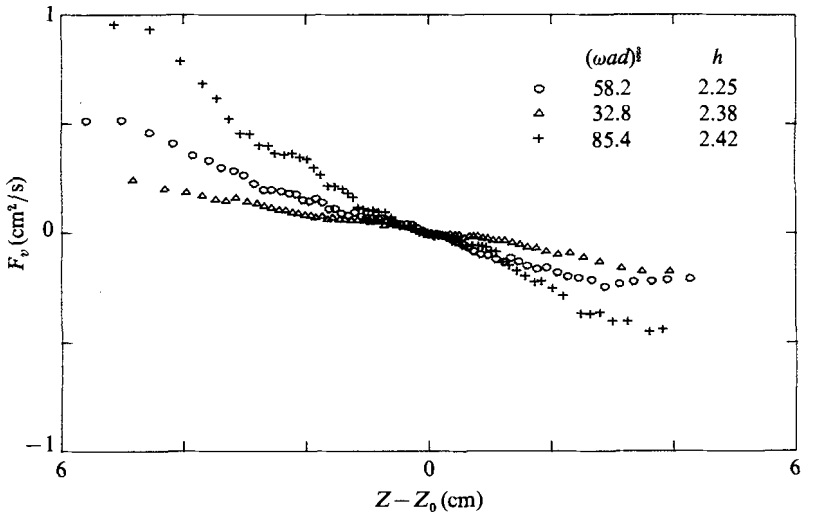

FIGURE 11. Three unscaled measurements of volume transport profiles: ○, experiment 15, profile 5; △, 19 and 5; +, 20 and 3, respectively.

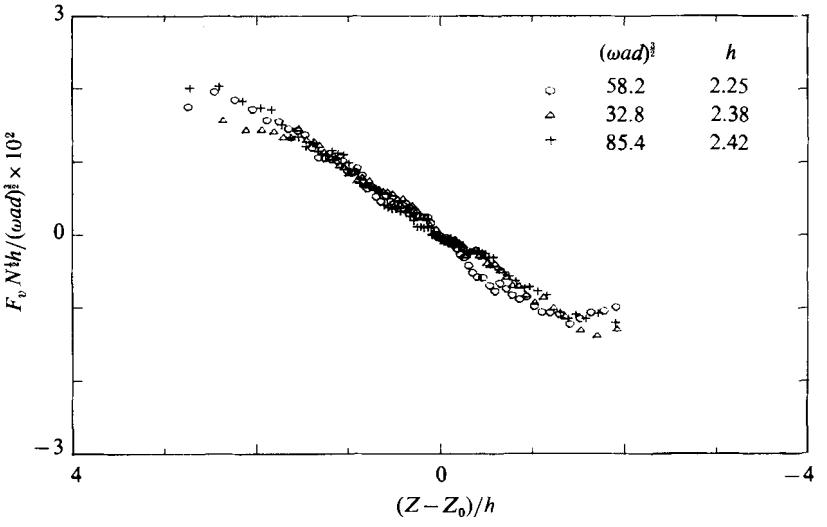

FIGURE 12. The same three profiles as in figure 11, scaled according to equation (4.19).

of isopycnals between successive probe traverses. If $\zeta(\rho, t)$ is the height of the fluid in the interior with density ρ at time t, then the change in volume above this isopycnal surface in the time interval t_1 to t_2 is

$$\Delta V = \{\zeta(\rho, t_1) - \zeta(\rho, t_2)\}\, L(\zeta_m),$$

where

$$\zeta_m = \tfrac{1}{2}\{\zeta(\rho, t_1) + \zeta(\rho, t_2)\}.$$

and $L(\zeta)$ is the length of the region of ambient fluid at this height. Consequently, the volume transport at ζ_m was estimated as

$$F_v = \frac{\Delta V}{t_2 - t_1}.$$

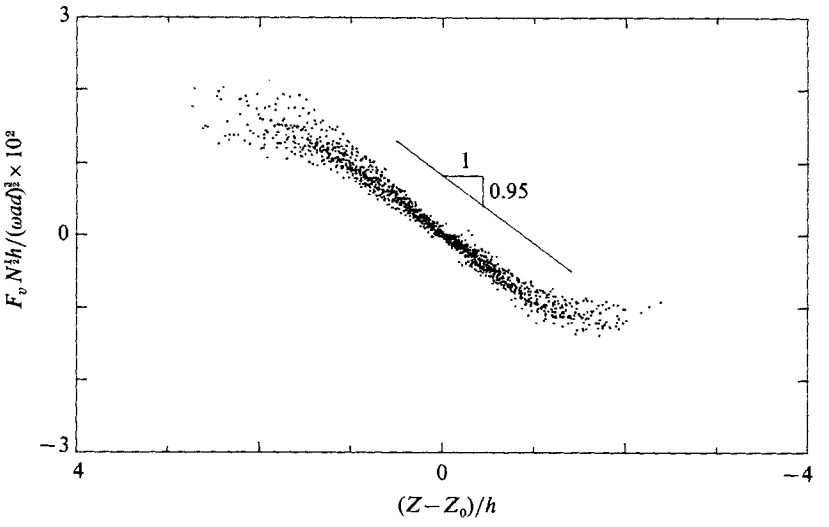

FIGURE 13. A summary diagram of the scaled volume fluxes in all sets of experiments.

For this calculation, the profiles were re-digitized at equal intervals of ρ, and three of the individual distributions of F_v are shown in figure 11. Figure 12 shows the collapse of these data under the scaling (4.19) and figure 13 includes all measurements in this series of experiments. The close grouping of the data does give confidence that the scaling (4.19) is appropriate for the experiments and the linearity of F_v with depth is evident over the range $|Z-Z_0|/h \lesssim 1$ over which the ambient fluid is significantly stratified. When $|Z-Z_0|/h$ is greater than about 1.5, the scatter of the results can be seen to increase. In these regions where the density gradient is small, the errors in measuring the isopycnal displacements become larger. In addition, at the top and bottom of the tank, which are not at fixed values of $(Z-Z_0)/h$, F_v must of course vanish so that the measured profiles must diverge from (4.19) as $(Z-Z_0)/h$ increases, as they do. From figure 13, we find the constant of proportionality between the scaled volume transport and $(Z-Z_0)/h$ to be 9.5×10^{-3}, a magnitude in general accordance with our previous expectations. If we restore the slope factors as in (4.19) these direct measurements of F_v give $A = 6.2 \times 10^{-4}$.

The variation of this volume transport along the sloping boundary layer produces the intrusion into the ambient fluid. The intrusion velocity

$$v_{\mathrm{I}} = \frac{\partial F_v}{\partial Z} = 6.2 \times 10^{-4} \frac{\cos^2\theta}{(\sin\theta)^{\frac{3}{2}}} \frac{(\omega ad)^{\frac{3}{2}}}{N^{\frac{1}{2}}h^2}, \tag{4.20}$$

$$= 9.5 \times 10^{-3} \frac{(\omega ad)^{\frac{3}{2}}}{N^{\frac{1}{2}}h^2} \tag{4.21}$$

(the latter giving the measured coefficient for this slope) and is expected to be almost uniform throughout the stratified layer in the range $|Z-Z_0|/h < 1$. The movements of initially vertical dye traces were observed many times during the experiments, typical examples being shown in figures 14 and 15. In the upper and lower unstratified layers, fluid moved towards the sloping bed to be entrained into the boundary layer. The flow in the stratified layer was away from the sloping bed with relatively thin shear layers separating the counterflowing streams. At the start of

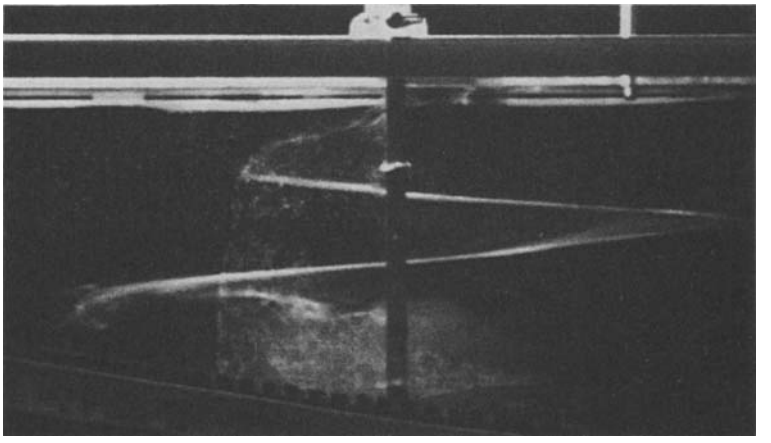

FIGURE 14. Fluorescein dye traces showing the vertical velocity profiles in the interior at the beginning of the experiment, with a thin pycnocline. The sloping bed is to the left and the motion towards the right (away from the boundary layer) is over the depth interval where the fluid is stratified. Unstratified fluid above and below moves to the left towards the boundary layer.

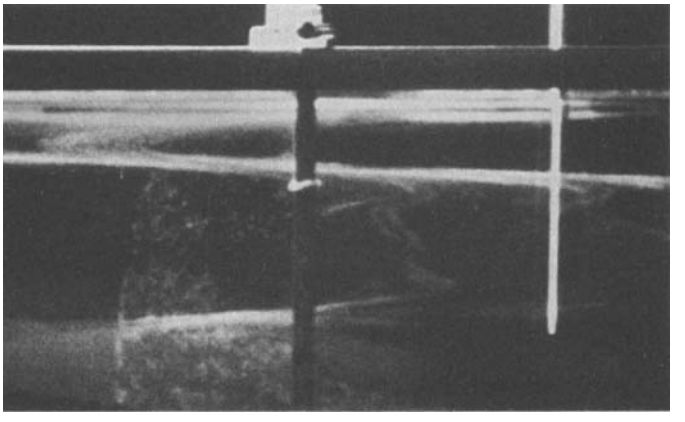

FIGURE 15. Following figure 14, later in the experiment, when the pycnocline is more diffuse, the intrusion velocity profile is approximately uniform throughout the depth of the pycnocline; above and below the stratified region, fluid continues to move towards the boundary layer to be entrained.

each experiment, when the pycnocline was thin, the intrusion was jet-like but broadened relatively rapidly as the isopycnals separated. The velocity profile of the intruding flow then became fairly flat as soon as the depth h of the stratified layer exceeded a couple of boundary-layer thicknesses, though irregularities of the order of 20 % of the mean were generally to be seen. The detailed profile of the irregularities did not seem to be repeatable from one experiment to the next, nor did they persist unchanged throughout the course of a single experiment as the stratified layer broadened. The boundary-layer flow is, after all, turbulent and the intrusion velocity is the *derivative* of the volume transport so that some randomness is to be expected. In contrast, the evolution of the density profiles reflects the time integral of the volume fluxes, so that these profiles remain smooth.

Finally, let us turn to the distribution with depth of the mass transport or, equivalently, buoyancy transport in the boundary layer. The results are presented most symmetrically if the reference density for buoyancy is taken as that at the level

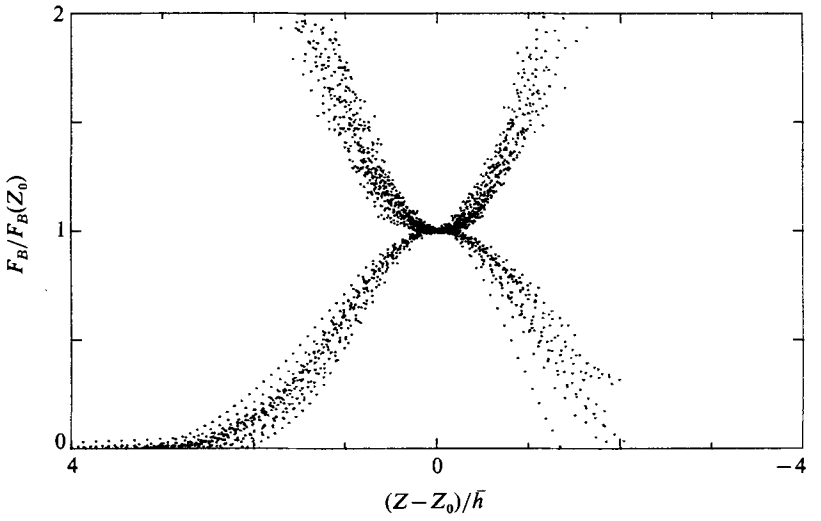

FIGURE 16. A summary of the mean distributions of total buoyancy transport in the boundary layer with $(Z-Z_0)/\bar{h}$, the reference value of zero buoyancy being taken as that at $Z=Z_0$, is given by the upper set of points. The lower set represents the contribution from turbulent dispersion in the boundary layer and the difference, the convective transport associated with the net volume flux.

Z_0 of zero volume flux. The diffusive buoyancy flux in the boundary layer is downwards, and with this choice of reference density the convective flux associated with the mean convergence is also negative, fluid with positive buoyancy in the upper half of the layer moving down, while in the lower half, fluid moving up the layer has negative buoyancy. The rate of change of buoyancy, integrated throughout the region of the tank above the height Z, is equal to the net buoyancy transport into the region across the level Z arising from (*a*) the diffusive and convective transports down the boundary layer and (*b*) the vertical convection in the interior region whose *volume* transport exactly balances that in the boundary layer:

$$\frac{\mathrm{d}}{\mathrm{d}t}\int_Z B(Z)\,\mathrm{d}A = \int_0^{L(Z)} B(Z)\,W\,\mathrm{d}X + F_{\mathrm{B}}(Z)$$
$$= -F_v(Z)\,B(Z) + F_{\mathrm{B}}(Z),$$

where W here represents the vertical velocity in the interior region and X is measured horizontally from the end of the tank. Consequently, the boundary-layer buoyancy transport can be expressed in terms of quantities measured in the interior ambient fluid:

$$F_{\mathrm{B}}(Z) = \frac{\mathrm{d}}{\mathrm{d}t}\int_Z B(Z)\,\mathrm{d}A + F_v(Z)\,B(Z). \tag{4.22}$$

The integral in the first term was calculated from the experimental data in the same manner as described earlier (cf. (4.12)).

In the boundary layer itself, the total buoyancy transport is the sum of the turbulent diffusive transport and the convective transport associated with the convergent mean flow. The variations in mean buoyancy along the boundary layer extend over a somewhat greater depth range than in the ambient fluid, so that the mean buoyancy in the boundary layer $\overline{B}$ at a given depth is somewhat different from that outside. However, as the profiles of figure 7 indicate, the differences are small

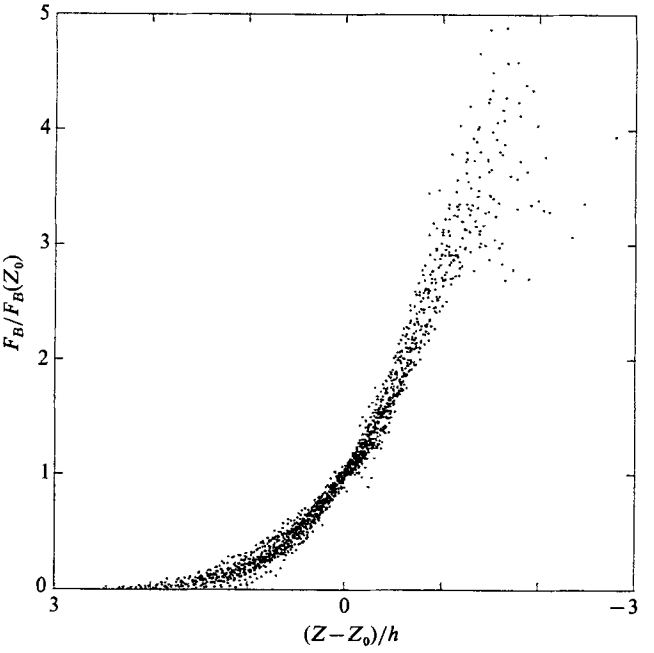

FIGURE 17. The distribution of transport of buoyancy relative to that in the surface layer (or equivalently, the transport of salt) as a function of $(Z-Z_0)/h$.

compared with the total range of buoyancy in the fluid so that the second term in (4.22) is closely equal to the convective transport of buoyancy in the boundary layer and, by default, the first is closely equal to the turbulent diffusive flux. These two terms are shown separately in figure 16 as functions of $(Z-Z_0)/h$. At the top and bottom of the pycnocline, the fluxes are dominantly convective and they are entirely diffusive at $Z = Z_0$. The downwards flux of buoyancy in the top half of the layer decreases in magnitude as fluid, buoyant with respect to that at the midpoint $Z = Z_0$, intrudes into the interior. Likewise, below the level Z_0, the upwards transport of negative buoyancy decreases with decreasing depth to compensate for the intrusion of fluid with negative buoyancy into the ambient interior.

A more conventional representation of the distribution of buoyancy transport is given in figure 17 in which the surface fluid is taken as having zero buoyancy. Since the points are normalized with respect to the transport at $Z = Z_0$, this can equally be interpreted as the boundary-layer salt transport, and it is easier to think of it in these terms. At the upper edge of the pycnocline, the volume transport downwards carries no salt so that the vertical salt transport vanishes. At $Z = Z_0$, the volume transport vanishes so that the ratio is unity, while at the bottom of the pycnocline, the transport is again entirely convective. This distribution of transport does not have the symmetry of figure 16 since the process involves both turbulent diffusion and convection – in the upper part of the pycnocline the convection opposes the dispersion, while in the lower part these two components of the transport are in the same direction, upwards. When $|Z-Z_0|/h$ is greater than approximately 1.5, the measurements of volume flux are inaccurate for the reasons mentioned earlier and the points show considerable scatter. The actual flux does not, of course, rise indefinitely as $(Z-Z_0)/h$ increases, the true value at the bottom of the pycnocline having a value of apparently about $4F_B(Z_0)$.

5. Transports in terms of boundary-layer parameters

The smallness of the numerical coefficients such as those in (4.14) and (4.15) might initially be a source of puzzlement, since the scaling arguments should lead to coefficients that are generally of order unity. The reason, it appears, lies in the relative inefficiency of the oscillating bed as a turbulence generator when the scale velocity is expressed as ωa, the maximum speed in the oscillation. In the somewhat analogous laminar creeping flow along a sloping boundary of a stratified fluid as considered by one of the authors (Phillips 1970), the boundary-layer thickness

$$\delta = \left(\frac{4\nu\kappa}{N^2 \sin^2\theta}\right)^{\frac{1}{4}}, \tag{5.1}$$

where ν and κ are the molecular viscosity and diffusivity, constant throughout the fluid in that situation. In the present turbulent flow, the fluxes of salt and momentum are confined to the boundary layer, but a comparison of (5.1) and (4.7), neglecting the virtual origin, indicates that the effective eddy viscosity (and eddy diffusivity, both being approximately equal in the turbulent flow) is

$$\nu_e, \kappa_e \approx 1.3 \times 10^{-2}\, \omega a d. \tag{5.2}$$

Our observations of the shadowgraph images do confirm that the scale of the largest eddies in the pycnocline boundary layer is of the order of d, but the characteristic velocities of the eddies are numerically considerably smaller than ωa. This product does apparently determine the velocity scale, though it is numerically much larger; just as in an ordinary rough boundary layer, the mean stream velocity determines the friction velocity u_* characteristic of the turbulence, though again it is numerically much larger.

The Reynolds number of the turbulent fluctuations in the experimental flow can be expressed in various ways. The ratio $\omega a d/\nu$ is of the order 500–2000, but the Reynolds number may be better defined as the ratio of the eddy viscosity to the molecular value. In all experiments of this kind this latter ratio is unfortunately small, and of the order 20 in these experiments, giving a ratio of energy-containing to dissipative lengthscales of only about 10.

If the fluxes are expressed in terms of the inferred eddy viscosity (5.2), the numerical coefficients are indeed found to be of order unity. From (4.14),

$$F_B(Z_0) = 0.60 \left\{\frac{\nu_e N(Z_0)}{\sin\theta}\right\}^{\frac{3}{2}} \cos^2\theta, \tag{5.3}$$

while from (4.15)

$$K_y = 0.29\, \nu_e \cot^2\theta. \tag{5.4}$$

The volume flux (4.19) is expressed, for an approximately Gaussian distribution of $N^2(Z)$, as

$$F_v(Z) = 0.42\, \frac{\nu_e^{\frac{3}{2}}}{N^{\frac{1}{2}} L}\, \frac{\cos^2\theta}{(\sin\theta)^{\frac{3}{2}}}\, \frac{Z - Z_0}{h} \tag{5.5}$$

and the intrusion velocity

$$v_I = 0.42\, \frac{\nu_e^{\frac{3}{2}}}{N^{\frac{1}{2}} h^2}\, \frac{\cos^2\theta}{(\sin\theta)^{\frac{3}{2}}}. \tag{5.6}$$

As the slope θ of the bed decreases, these expressions suggest that the intrusions and mean circulations become more vigorous, though the description given here must fail as $\theta \to 0$. It is not yet clear precisely how this failure occurs, but when $\theta = 0$ the geometry reduces to the entrainment of a turbulent bottom boundary layer into

stratified fluid above, in which there is no quasi-steady state, the boundary-layer thickness continually increasing with time. The limiting behaviour at small θ of this intrusive circulation remains to be explored.

6. Some field indications of boundary mixing

These experiments clearly suggest that, when longitudinal mean or tidal flows are maintained in an estuary or along a sloping bottom, the water column being stratified non-uniformly, then a mean lateral circulation develops with an intrusion in the strongly stratified layer leaving the boundary region and moving into the interior. In the case of an estuary of finite width, this leads to a lateral convergence of the fluid in the stratified layer with a lateral divergence in more homogeneous regions above and below. A passive contaminant placed in the pycnocline region will be confined laterally, the mean convergence opposing dispersion along isopycnal surfaces, while one injected near the surface will spread laterally more rapidly in response to the divergence. Some recent interesting observations in the northern Chesapeake Bay by Tyler (1984), though made primarily to study the dispersion of dinoflagellates, do appear to be consistent with this expectation.

Rhodamine dye was injected into the lower part of the pycnocline at a point just south of the Chesapeake Bay Bridge near the centre of the estuary and traced for a period of six days. Figure 18(*a*) shows the location of the dye mass on 7 May 1980, six hours after injection, while figure 18(*b*, *c*) gives contours, expressed in parts per billion (p.p.b.), two and four days later. The dye patch is clearly dispersed along the estuary, the spreading enhanced by the longitudinal shear, with local concentration maxima eventually entering the Patapsco River channel to the north-west and the Chester River to the east. Remarkably, however, the lateral dispersion along isopycnal surfaces in the pycnocline is extremely slow. Current meters, moored across the section of the bay at 38° 58′ 25″ N provided the distribution of mean isotachs in the axial direction shown in figure 19(*a*), with maximum mean speeds near the eastern slope. Superimposed on these mean velocities are, of course, the tidal current oscillations of comparable magnitude, which do not vary greatly with depth in this region. The lateral distribution of isopycnals, contours of σ_t, on 11 May (unfortunately a couple of miles further south) is shown in figure 19(*c*) and indicates a maximum density gradient near the eastern shore at a depth of about 10 m, becoming more diffuse towards the western slope. The distribution of mean isotachs for the cross-axis flow is shown in figure 19(*b*) and it is noteworthy that relatively high lateral velocities leave the eastern shore where the stratification of the pycnocline is greatest and the axial velocities largest. By 11 May, most of the dye had been carried to the north, as shown in figure 18(*c*), but the dye remaining at this section is shown in figure 19(*c*) to have been carried away from the more energetic eastern shore towards the west, some being entrained into the surface mixed layer but no detectable amounts being mixed along the isopycnals to the east.

Another set of measurements reported by Churchill (1985) was made in near-shore waters off the southern coast of Long Island. A moored current-meter array along a line normal to the (almost linear) shore line measured offshore and alongshore velocity components while hydrograph surveys provided the average density field during the measurement intervals. During March 1978, the water column was nearly homogeneous; mean alongshore currents at the first mooring 3 km from the shore were in the range 7–9 cm/s while the mean offshore currents were weak (0.4–1.9 cm/s)

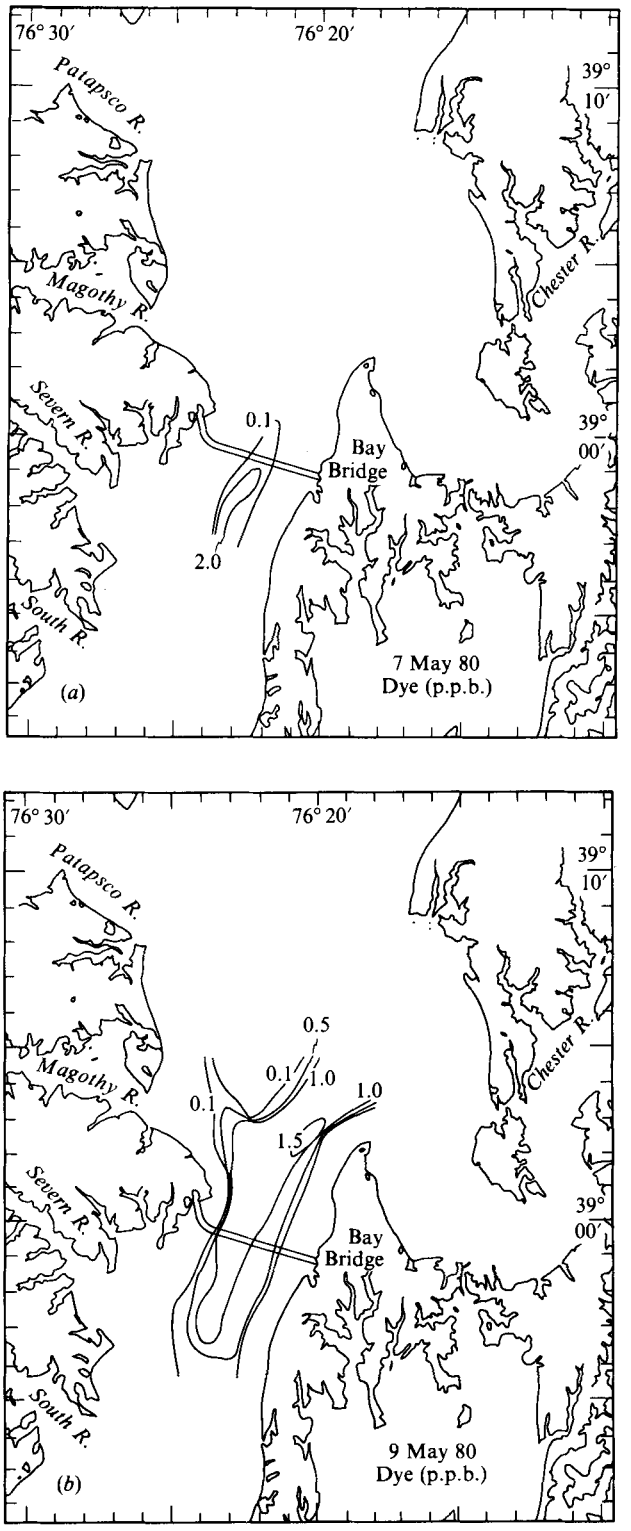

FIGURE 18 (*a*, *b*). For caption see facing page.

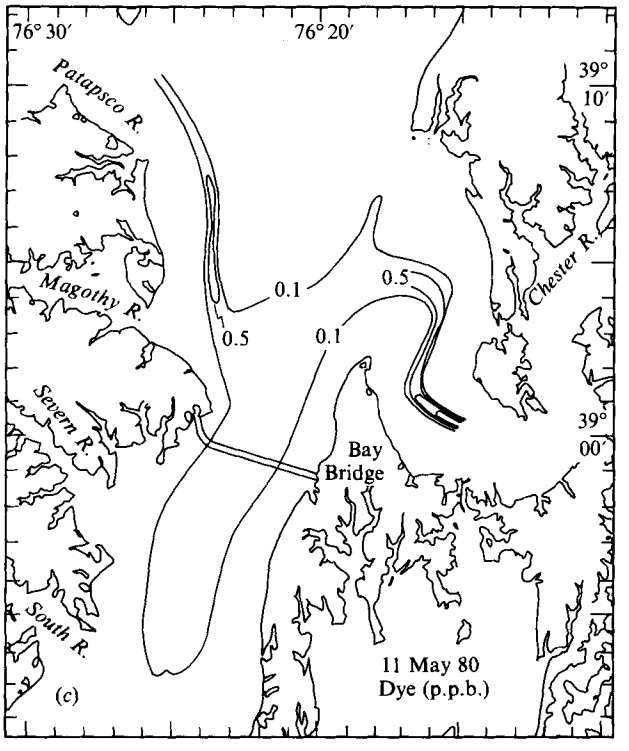

FIGURE 18. Location of dye masses measured by Dr Tyler in the Chesapeake Bay, following a release just south of the Bay Bridge. Rhodamine concentrations in p.p.b. (*a*) 7 May 1980, six hours after injection. (*b*) 9 May and (*c*) 11 May.

and variable with depth. During May 1977 and August 1978, however, during periods of generally negligible wind stress, the water column was highly stratified and the alongshore current perhaps somewhat larger (8 cm/s at the first mooring to 12–16 cm/s at the third, 9 km offshore) but the offshore currents were both larger in magnitude and consistent in pattern. During these intervals the stratification persisted to within about 4 m of the surface and measurements in the top 10 m showed offshore velocities generally in the range 4–8 cm/s. At greater depths, the lateral velocities were generally onshore but smaller in magnitude. This general pattern again seems consistent with a pattern of intrusions set up by boundary mixing. Churchill noted the existence of alongshore density gradients and attributed the cross-shore flow to them, but the relation between the two can hardly be considered causal. A rough geostrophic balance will tend to associate a longitudinal density gradient with a mean lateral flow; we would interpret the boundary-layer mixing as generating the lateral flow while the alongshore pressure gradient develops in approximate geostrophic adjustment.

These various observations, while highly suggestive, can hardly be considered definitive. The data are sparse and quantitative comparisons are not yet possible. The effective eddy viscosity in the slope boundary layer is not known in either case; it is likely to depend more on the mean square or the absolute value of the alongshore velocity than the mean. It is to be hoped that those indications that we already have will however stimulate more detailed field measurements of this kind.

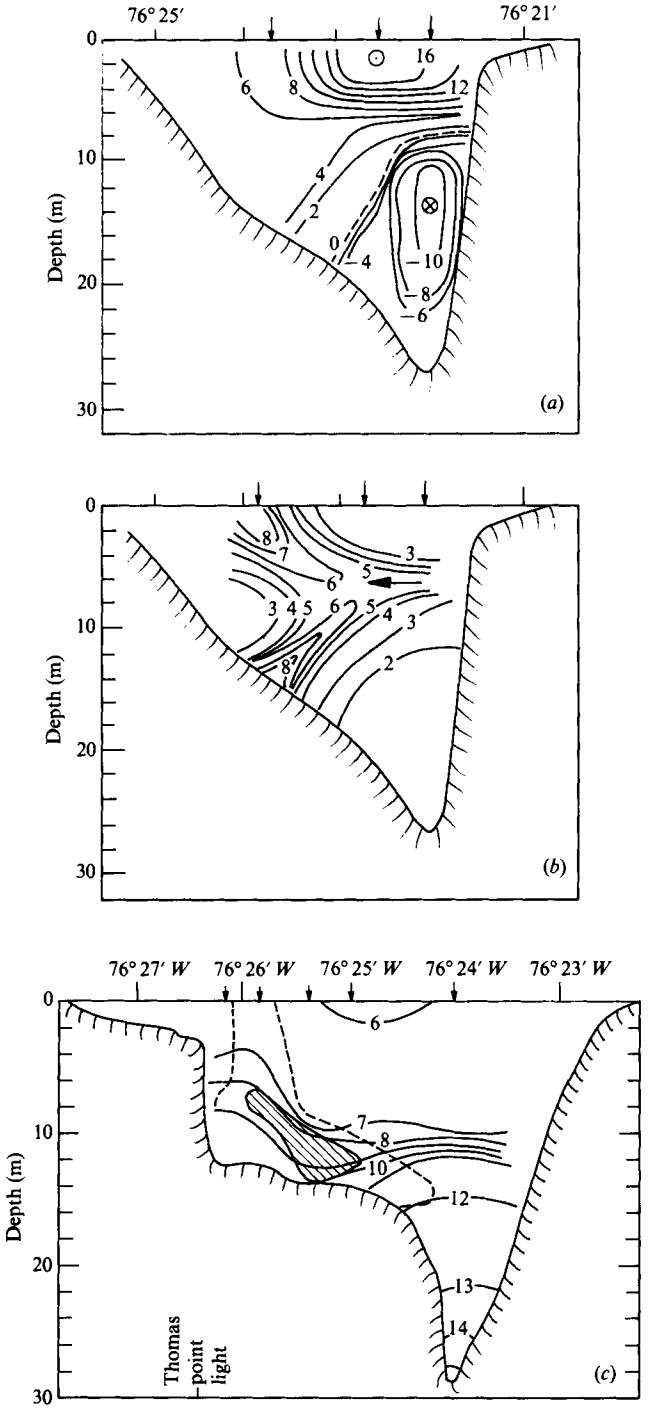

FIGURE 19. Cross-section of the velocity distributions through the Chesapeake Bay at latitude 38° 58′ 25″ N, 1–14 May 1980. From Tyler (1984). (*a*) gives mean isotachs along the axis and (*b*) those across the axis (cm/s). (*c*) shows density isopleths (σ_t) on 11 May across a section at 38° 54′ N with dye concentrations above 0.1 p.p.b. shaded and above 0.05 p.p.b. enclosed by the broken line. Note the lateral intruding flow from the energetic eastern shore in the depth range of high stratification.

This research was supported by the National Science Foundation under grant no. OCE 8405306 and a preliminary account was given at the IUTAM Symposium on mixing and stratified fluids at Margaret River, Western Australia in August 1985. The authors are most grateful to Mr Yign Noh for assistance with the experiments and to Dr Mary Tyler for providing the data on the Chesapeake Bay experiment.

REFERENCES

BATCHELOR, G. K., BINNIE, A. M. & PHILLIPS, O. M. 1955 The mean velocity of discrete particles in turbulent flow in a pipe. *Proc. Phys. Soc.* B **68**, 1095–1104.

CHURCHILL, J. H. 1985 Properties of flow within the coastal boundary layer off Long Island, New York. *J. Phys. Oceanogr.* **15**, 898–916.

ERICKSEN, C. C. 1985 Implications of ocean bottom reflection for internal wave spectra and mixing. *J. Phys. Oceanogr.* **15**, 1145–1156.

IVEY, G. N. & CORCOS, G. M. 1982 Boundary mixing in a stratified fluid. *J. Fluid Mech.* **121**, 1–26.

MUNK, W. H. 1966 Abyssal recipes. *Deep-Sea Res.* **13**, 707–730.

OLSON, P. L., BOICOURT, W. C. & NAJARIAN, T. O. 1982 A hydrodynamic study of the Baltimore Harbor System, Part II. A numerical model of the Baltimore Harbor Circulation. *Chesapeake Bay Inst. Bulletin no.* 2. 152 pp.

PHILLIPS, O. M. 1970 On flows induced by diffusion in a stably stratified fluid. *Deep-Sea Res.* **17**, 435–443.

STIGEBRANDT, A. 1976 Vertical diffusion driven by internal waves in a sill fjord. *J. Phys. Oceanogr* **6**, 486–495.

THORPE, S. A. 1982 On the layer produced by rapidly oscillating a vertical grid in a uniformly stratified fluid. *J. Fluid Mech.* **124**, 391–410.

TOWNSEND, A. A. 1956 *The Structure of Turbulent Shear Flow.* Cambridge University Press. 315 pp.

TURNER, J. S. 1979 *Buoyancy Effects in Fluids.* Cambridge University Press. 368 pp.

TYLER, M. A. 1984 Dye tracing of a subsurface chlorophyll maximum of a red-tide dinoflagellate to surface frontal regions. *Mar. Biol.* **78**, 285–300.

WUNSCH, C. 1970 On oceanic boundary mixing. *Deep-Sea Res.* **17**, 293–301.

WUNSCH, C. & HENDRY, R. 1972 Array measurements of the bottom boundary layer and the internal wave field on the continental slope. *Geophys. Fluid Dyn.* **4**, 101–145.